24th EUROPEAN ROTORCRAFT FORUM
Marseilles, France - 15th - 17th September 1998

FM 03

EFFECTS OF ROTOR DISC - TILT ON HELICOPTER PILOTED SIMULATION

M.D. Pavel
Faculty of Aerospace Engineering
Delft University of Technology

SUMMARY

This paper investigates the effects of including the flapping dynamics in a piloted simulation model. Two questions are to be analyzed:
1) whether modeling the blade disc-tilt dynamics is essential in a piloted simulation model and,
2) what is the effect on the piloted simulation of different approximations in the analytical expressions of the flapping angles.
As concerns the first question, time-domain simulations are performed with fully coupled non-linear body-flap models. First, a six degrees of freedom (dof) non-linear body model is developed and used to simulate two mission tasks (a deceleration and a side-step manoeuvre) with two helicopters - Puma SA330 articulated rotor helicopter and Bo105 semi-rigid rotor helicopter - chosen because of their different rotor configuration. In order to study the influence of the blade disc-tilt dynamics on the piloted simulation, the six dof model is then extended, first including only the low frequency regressing flapping mode (resulting in the so called "eight dof model") and then including also the high frequency advancing flapping mode (resulting in the so called "nine dof model") in the piloted simulation model. With respect to the regressing flapping mode, it is found that this mode influences the simulation results of the deceleration and side-step manoeuvres performed with the Bo105 semi-rigid rotor helicopter. This result confirms the predictions made in a previous study [1] where, using the analysis in the complex plane, it was also found that a semi-rigid rotor helicopter does require a coupled flap-body model for piloted simulation. Simulating the two manoeuvres with the Puma helicopter as well, it is found that the regressing flap mode has no influence on the deceleration manoeuvre but does influence the results of the side-step manoeuvre. Therefore, the effects of the flapping dynamics on the piloted simulation depend not only on the rotor configuration but also on the manoeuvre performed. As to the advancing flapping mode, it is found that this mode neither influences the simulation results of the deceleration manoeuvre performed with the Bo105 semi-rigid rotor helicopter nor with the Puma articulated rotor helicopter, confirming once again the predictions made in [1]. Concerning the second question, using three different approximations in the analytical expressions of the steady-state flapping angles to simulate the deceleration manoeuvre with the Bo105 shows that the high-order coupling terms in the analytical expressions of the flapping angles do influence the piloted simulation results. The paper ends with some recommendations on how to proceed further in order to predict when the flapping dynamics should be included in the piloted simulation model.

NOMENCLATURE

I_x	helicopter moment of inertia about body x-axis [kg m^2]
I_y	helicopter moment of inertia about body y-axis [kg m^2]
I_z	helicopter moment of inertia about body z-axis [kg m^2]
I_{xz}	helicopter product of inertia about body x and z-axes [kg m^2]
I_{bl}	inertia moment of the blade section [m^4]
m	helicopter mass [kg]
h	hub position relative to z axis [m]
$p, \bar{p}$	helicopter roll angular velocity [rad/s] and

its non-dimensional value [-]

$q, \bar{q}$ helicopter pitch angular velocity [rad/s] and its non-dimensional value [-]

$r, \bar{r}$ helicopter yaw angular velocity [rad/s] and its non-dimensional value [-]

R rotor radius [m]

r_{bl} current rotor radius [m]

u component of airspeed along body x-axis [m/s]

v component of airspeed along body y-axis [m/s]

w component of airspeed along body z-axis [m/s]

V total helicopter velocity [m/s]

x position along Earth X-axis [m]

x_{des} desired helicopter longitudinal position [m]

y position along Earth Y-axis [m]

y_{des} desired helicopter lateral position [m]

z position along Earth Z-axis [m]

Θ Euler pitch angle [rad]

Θ_{des} desired pitch angle [rad]

Ψ heading angle [rad]

Ψ_{des} desired heading angle [rad]

Φ Euler roll angle [rad]

Φ_{des} desired roll angle [rad]

c helicopter climb velocity [m/s]

c_{des} desired climb speed [m/s]

h helicopter altitude [m]

h_{des} desired altitude [m]

θ_0 collective pitch [rad]

θ_{1c} lateral cyclic pitch [rad] $\theta_{1c} > 0$ for pilot stick to the right for the counter-clockwise helicopter, and to the left for the clockwise helicopter

θ_{1s} longitudinal cyclic pitch [rad] $\theta_{1s} > 0$ for stick forwards

θ_{0tr} tailrotor collective [rad]

$\beta(t) = a_0(t) - a_1(t)\cos\psi - b_1(t)\sin\psi$ blade flapping angle[rad]

Ω rotor rotational speed [rad/sec]

$\nu^2 = 1 + K_\beta/(I_{bl}\Omega^2)$ non-dimensional natural frequency of the flap motion

λ_0 normalised uniform inflow velocity [-]

ψ azimuth angle [rad]

γ Lock number [-]

1. INTRODUCTION

Simulators are nowadays an important tool in training helicopter crews, accounting for 50% of total training time. A high level of motion simulation fidelity is therefore of paramount importance. As the development of high-fidelity mathematical models of helicopters continues, it is often tempting for the simulation developer to continue to add complexity to the model, without analysing the necessity for this complexity. Therefore, some guidelines relative to the necessary detail of the piloted simulation model are still needed, before starting the actual derivation of the dynamic equations of motion.

A previous ERF paper [1] presented some investigations taking place at Delft University of Technology relative to the question of necessary model approximation within the framework of the new simulator (SIMONA) which is being built at present. A formal method has been described which can be used to determine the type and number of the relevant degrees of freedom essential to be included in a simulation model. The method consisted mainly on an analysis in the complex plane of the relative position between the body and rotor dynamics. The predictions made using this procedure were first exemplified for the investigation of the coupled body-flapping motion. The results in the complex plane showed that coupling effects between flap and body motion seem to be of importance in a piloted simulation model for the hingeless helicopter BO 105.
The aim of the present paper is to investigate the influence of the flapping dynamics on the body motion in the time-domain, in order to validate the mentioned predictions. The paper is divided in two parts: the first part in which different body-flap models are investigated in order to determine the influence of the blade disc-tilt dynamics on the piloted simulation model and the second part to determine if different approximations of the analytical expressions of the flapping angles have any influence on the piloted simulation model.

2. PRELIMINARIES

This chapter gives a summary of the prediction procedure reported earlier in [1]. The method can be used as a criterion to reveal how many degrees of freedom of rotor dynamics are necessary to be included in a helicopter simulation model. The procedure in essence involves the study of the uncoupled body and rotor modes. The proposed method goes through the following steps:
(1) regarding the helicopter as a summation of mutually uncoupled subsystems, the equations of motion for every uncoupled deflection mode are derived,
(2) solving the formulated equations of motion, the eigenmodes of the motion are obtained,
(3) the eigenvalues of the uncoupled motion of the

subsystems are represented in the complex plane. For the representation of the eigenvalues of the rotating subsystems, the Coleman transformation is used so that the new eigenfrequencies of the rotating systems can be directly compared with the eigenfrequencies of the non-rotating components. (4) using the representation in the complex plane, the "critical regions" are defined. A "critical region" is defined as an area of the complex plane where potential couplings between different modes occur-within and between subsystems. The criterion for a critical region is the relative position of the poles in the complex plane, i.e. if the poles in the complex plane associated with the uncoupled motion of different deflection modes are close together, one may expect that these modes will couple together. (5) Conclusions concerning the degrees of freedom to be used in the structural model can now be drawn on the basis of the results obtained. It is only after having performed such a relatively simple exploratory analysis, that one should proceed and write out the fully coupled, non-linear model that has been determined to be relevant in the case considered.

Applying the described method to the rigid flapping motion, it appeared that the semi-rigid rotor systems do require some form of coupled flap-body motion models, a result revealed also in literature [9,10]. This paper investigates this result in the time-domain, by considering two typical manoeuvres, and investigating the effects of the tip-path-plane dynamics on the simulation results.

3. SIX DEGREES OF FREEDOM BODY MODEL FOR PILOTED FLIGHT SIMULATION

A general six degrees of freedom non-linear rigid body model is first developed as a basic model to be used for the piloted time-domain simulations.

3.1 Model Description

In a typical six degrees of freedom model, the helicopter motion is represented by three translations and 3 rotations around the body axis-system of unit vector $\{\bar{E}_b\}=\{\bar{i}\ \ \bar{j}\ \ \bar{k}\}^T$ (see fig.1).

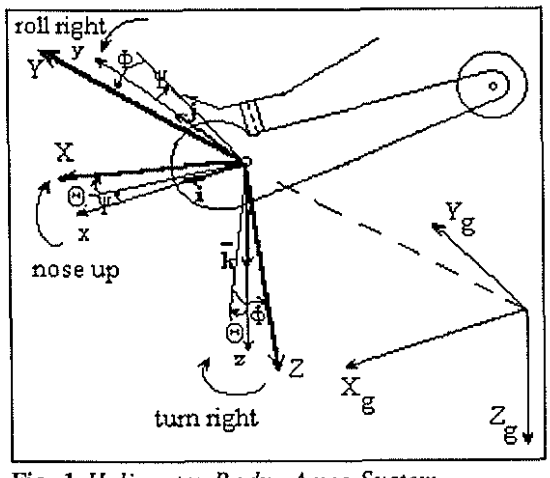

Fig. 1 *Helicopter Body- Axes System*

The helicopter body is modeled dividing the helicopter in its main components: rotor, fuselage, tailrotor, horizontal stabilizer, vertical fin and summing the contribution of each part to the general system of forces and moments. The following assumptions are made:
- aerodynamic forces and moments are calculated using analytical blade element theory,
- rotor flapping is modeled using analytical steady-state flapping equations,
- the tailrotor is modeled as an actuator disc,
- the fuselage, horizontal and vertical tails are modeled with linear aerodynamics,
- rotor inflow is assumed to be uniform.

The helicopter body equations of motion are the fundamental equations of dynamics written in the body-axes system:

$$(\dot{u}\ \dot{v}\ \dot{w})[\,m\,]\{\bar{E}_b\}+(u\ v\ w)[\,m\,][\,\omega_x\,]\{\bar{E}_b\}=\left(F_R+F_{fus}+F_{tr}+F_{hs}+F_{fin}\right)\{\bar{E}_b\} \quad (7)$$

$$(\dot{p}\ \dot{q}\ \dot{r})[\,J\,]\{\bar{E}_b\}+(p\ q\ r)[\,J\,][\,\omega_x\,]\{\bar{E}_b\}=\left(M_R+M_{fus}+M_{tr}+M_{hs}+M_{fin}\right)\{\bar{E}_b\} \quad (8)$$

where:

$$[m]=\begin{bmatrix} m & 0 & 0 \\ 0 & m & 0 \\ 0 & 0 & m \end{bmatrix}$$ mass matrix

$$[J]=\begin{bmatrix} I_x & 0 & -I_{xz} \\ 0 & I_y & 0 \\ -I_{xz} & 0 & I_z \end{bmatrix}$$ moment of inertia matrix

$$[\omega_x]=\begin{bmatrix}0 & r & -q\\ -r & 0 & p\\ q & -p & 0\end{bmatrix}$$

F_R, F_{fus}, F_{tr}, F_{ht}, F_{fin},
M_R, M_{fus}, M_{tr}, M_{ht}, M_{fin} are the external forces and moments acting on the helicopter components.

For a complete derivation of the forces and moments in the relations (1), (2), the reader is referred to [2, 1]. Appendix A, equations (A.1÷A.6), gives the final form of the helicopter equations of motion implemented in the six dof model developed in this paper. In order to describe the motion of the helicopter in an inertial system, the Euler equations (A.7÷A.9) and the equations of the helicopter trajectory (A.10÷A.12) need to be added to the general equations of motion (A.1÷A.6). Relations (A.1÷A.12) completely describe the helicopter motion in an inertial system of reference in the six degrees of freedom non-linear body model.

3.2 Modeling the dynamic inflow in the six degrees of freedom body model

In the 6 dof model developed in this paper, the dynamic inflow is considered as a separate degree of freedom. Two differential equations A.13 and A.14 - one for the main rotor inflow and the other for the tailrotor inflow - are added to the helicopter equations of motion, so that the variation of the inflow is calculated as a 'quasi-dynamic inflow' [3].

3.3 Modeling the pilot in the six degrees of freedom model

To fly the helicopter with the 6 dof model developed, a Stability Augmentation System (SAS) has to be implemented. For the manoeuvres used as example in this paper, four stabilization functions are developed, each one for each helicopter's control:

- Collective controls vertical speed

$$\theta_0=\theta_{0_{gm}}+K_c(c_{des}-c)+K_{corrc}\int_0^t(c_{des}-c)d\tau \qquad (3)$$

The desired vertical speed is controlled by an "altitude hold" controller, feeding back the height to the vertical speed:

$$c_{des}=K_h(h_{des}-h) \qquad (4)$$

- Longitudinal cyclic controls pitch attitude

$$\theta_{1s}=K_\Theta(\Theta-\Theta_{des})+K_q q+K_{\Theta corr}\int_0^t(\Theta-\Theta_{des})d\tau \qquad (5)$$

The desired pitch attitude is controlled by a "longitudinal position hold" controller:

$$\Theta_{des}=K_x(x_{des}-x)+K_u u+K_{xcorr}\int_0^t(x_{des}-x)d\tau \qquad (6)$$

- Lateral cyclic controls roll attitude

$$\theta_{1c}=K_\Phi(\Phi_{des}-\Phi)+K_p p+K_{\Phi corr}\int_0^t(\Phi_{des}-\Phi)d\tau \qquad (7)$$

The desired roll angle is controlled by a "lateral position hold" controller:

$$\Phi_{des}=K_y(y_{des}-y)+K_v v+K_{ycorr}\int_0^t(y_{des}-y)d\tau \qquad (8)$$

- Tailrotor collective controls heading angle

$$\theta_{0tr}=K_\Psi(\Psi_{des}-\Psi)+K_r r+K_{\Psi corr}\int_0^t(\Psi_{des}-\Psi)d\tau \qquad (9)$$

The desired yaw angle is controlled fast and smooth and does not need any proportional-integration-differentiation (PID) controller.
The six dof model presented here is used to investigate two mission tasks: a deceleration and a side-step manoeuvre, simulated with two different helicopters chosen mainly because of their different rotor configuration: the Puma SA330 having an articulated rotor and the Bo105 having a semi-rigid rotor.

4. DECELERATION MANOEUVRE

A deceleration-to-stop manoeuvre was simulated in horizontal cruising flight at 50m/s the helicopter has to be slowed down to hover within a distance of 2 km from the starting point, above a given point situated on the ground (see fig.2)

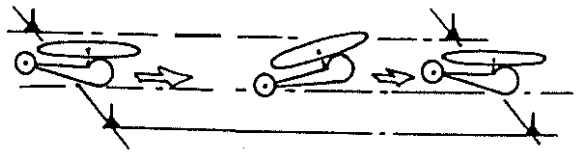

Fig. 2 *Deceleration Manoeuvre*

4.1 Flying the deceleration manoeuvre with the non-linear six degrees of freedom model

This paragraph presents the way the two exemplified helicopters, (Puma SA330, and Bo105) perform the deceleration manoeuvres with the 6 dof non-linear model.

Deceleration manoeuvre: Bo105

Figure 3 presents the way the pilot performs the manoeuvre with the two helicopters.

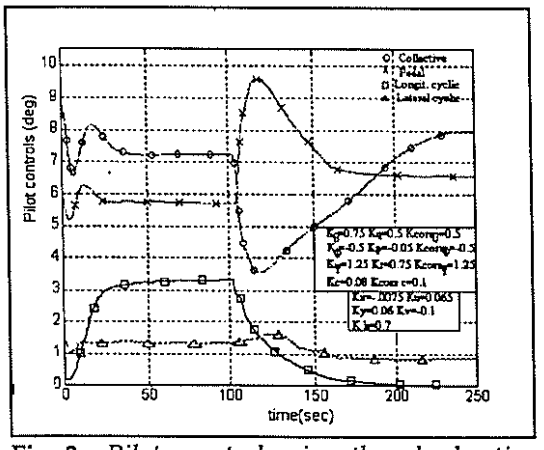

Fig. 3 *Pilot controls in the deceleration manoeuvre with Bo105, 6 dof model*

The following pilot actions can be read from the graphs:
With respect to the longitudinal cyclic: the pilot flies forwards the first 110 seconds and then gradually pulls back the stick in order to decelerate to the hover. The tip path plane tilts back, resulting in a tendency of the helicopter to climb. The longitudinal stick variation is closely related to the helicopter pitch attitude.
With respect to the collective, in the 110th second, the collective is lowered from 7.2 degrees to 3.6 degrees (this is in fact a reaction to the helicopter's climb tendency). After this, the collective is gradually increased to the hover trim position of 8 degrees.
With respect to the lateral cyclic, some action can be seen after 110 seconds when the stick is moved to the right- this action is simultaneous with the change in the roll angle to the left.
With respect to the pedal position, lowering the collective in the 110th second, an input in the right pedal is needed in order to correct the helicopter yaw motion (an input in collective causes a yaw rotation) . Then, as collective is increased in order to transit to the hover, the left pedal is applied.

Deceleration manoeuvre: Puma

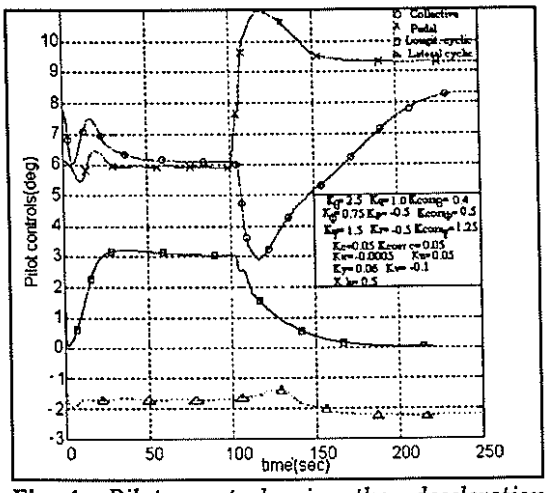

Fig. 4 *Pilot controls in the deceleration manoeuvre with Puma SA330, 6 dof model*

Looking at fig.4, the same actions of the pilot can be observed when performing the deceleration manoeuvre with the Puma. The only difference consists in the lateral cyclic. Because the Puma rotor rotates clockwise, the lateral cyclic is applied opposite from that of the Bo105-i.e. first to the left and then to the right. The gains used to simulate these manoeuvres are shown in fig. 4.

5. SIDE-STEP MANOEUVRE

This ADS-33 manoeuvre is described as consisting of the following stages: starting from hover, a first abrupt sidestep acceleration is carried out. After reaching the maximum allowable lateral speed, an abrupt deceleration back to hover is carried out. After hovering for 5 sec, the manoeuvre is repeated in the opposite direction.

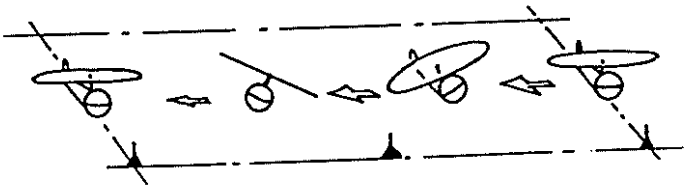

Fig. 5 *Side-step Manoeuvre*

Side-Step manoeuvre: Bo-105

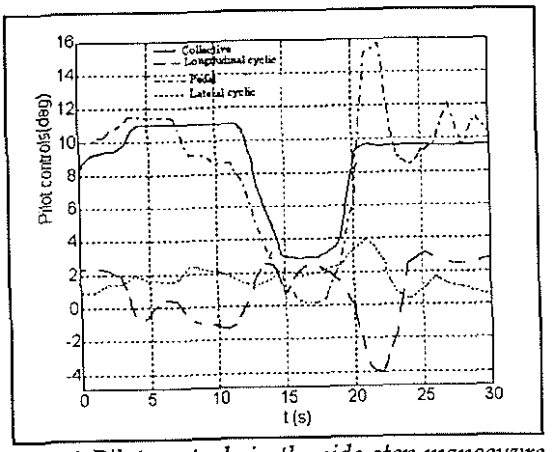

Fig. 6 *Pilot controls in the side-step manoeuvre with Bo105, 6 dof model*

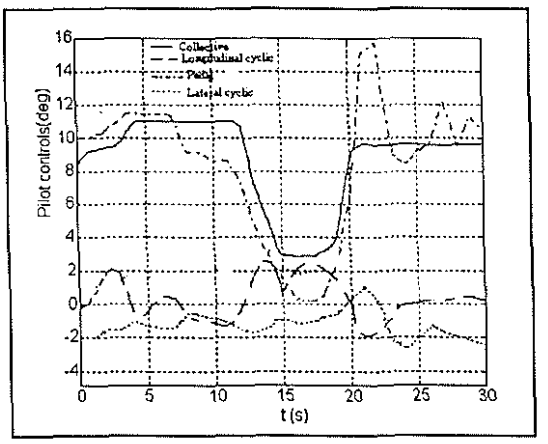

Fig. 7 *Pilot controls in the side-step manoeuvre with Puma, 6 dof model*

Gains used:

K_Θ=1.72 K_q=-0.57 $K_{corr\ \Theta}$=1.43
K_Φ=1.72 K_p=-0.57 $K_{corr\ \Phi}$=1.43
K_Ψ=1.72 K_r=-0.57 $K_{corr\ \Psi}$=1.43
K_c=0.06 $K_{corr\ c}$=0.05
K_x=-0.06 K_u=0.09
K_y=0.015 K_v=0.0225
K_h=0.015

With respect to lateral control, the lateral acceleration is initiated by moving the stick to the left. The acceleration is followed by a deceleration when the pilot moves the stick to the right. After hovering 5 sec the manoeuvre is repeated in the other direction. The amount of lateral stick can be correlated with the roll angle.
With respect to the longitudinal control: for the acceleration the stick is pushed firmly forward and then back in order to hover. In the deceleration phase, the stick is pulled back and then slightly pushed forward for the final hover.
With respect to the collective: in order to keep the altitude constant, the collective has to be increased first and then adjusted constantly.
With respect to the pedal: each movement in the collective results in a yawing motion which is corrected with the pedal.

Side-step manoeuvre: Puma

As for the side-step manoeuvre performed with the Bo105, the same pilot actions can be seen in fig.7 when the manoeuvre is simulated with Puma helicopter. For the simulation in fig. 7, the same gains as the one used above are used.

6. FLAPPING DYNAMICS

In order to determine the effects of flapping dynamics on the two manoeuvres described above, the flapping blade equation of motion in the rotating system needs first to be derived. This can be done by summing the moments due to the aerodynamic forces acting on the blade, the centrifugal force, Coriolis, inertia, and the restraint forces about the flapping hinge. The following assumptions are made in deriving the flapping motion:
- only rigid flap motion is considered,
- there is no elastic flapping, and no lag or pitch degree of freedom,
- the rotor is modelled with spring restraint and no flap hinge offset,
- the blade has constant chord and linear twist,
- the tip loss factor is assumed to be 1,
- the pitch-flap coupling is considered in the model by increasing the effective natural frequency of the flap motion [4, pp. 240],
- the effects of the aircraft motion on the blade flapping are limited to those due to the angular roll, pitch and yaw rate p, q, r (the angular accelerations are neglected),
- a uniform inflow is considered,
- root cutout and tip loss is neglected (effect reduced thrust)
- blade weight is neglected.

With these assumptions, the flapping equation in the rotating frame becomes:

$$\frac{\ddot{\beta}}{\Omega^2}+\beta\left(v^2-2\bar{r}\right)=2\bar{p}\cos\psi-2\bar{q}\sin\psi+\frac{M_a}{I_{bl}\Omega^2} \qquad (10)$$

The aerodynamic moment M_a is derived by

integrating the lift force over the span:

$$\frac{M_a}{I_{bl}\Omega^2}=\frac{\gamma}{2}\int_0^R\left(\theta\bar{U}_T^2-\bar{U}_T\bar{U}_P\right)\bar{r}_{bl}d\bar{r}_{bl} \qquad (11)$$

The tangential and perpendicular air velocity relative to the shaft plane are:

$$\bar{U}_T=\frac{u}{\Omega R}\sin\psi+\frac{v}{\Omega R}\cos\psi+\bar{r}_{bl}(1-\bar{r}) \qquad (12)$$

$$\bar{U}_P=\frac{u}{\Omega R}\beta\cos\psi-\frac{v}{\Omega R}\beta\sin\psi-\frac{w}{\Omega R}-\bar{r}_{bl}\times \times\left(\bar{q}\cos\psi+\bar{p}\sin\psi-\frac{\dot{\beta}}{\Omega}\right)+\lambda_0 \qquad (13)$$

Substituting these equations, the flapping equation in the rotating frame is deduced.

The equation of blade flapping motion associated with the rotating flapping angle is then transformed in the non-rotating body axis- system. This can be done in two ways:
- using the Coleman transformation [4] or,
- expressing the flapping angle in a first harmonic Fourier series of coefficients varying in time [5].
Reference 6 demonstrates that these two methods are equivalent, at least for a 3-and 4- bladed helicopter (the new coordinates of the flap motion in the non-rotating system obtained using the Coleman transformation correspond to the tip-path-plane coordinates as expressed in a first harmonic Fourier series used in the classical tip-path-plane approximation).

Transforming the flapping equations of motion from the rotating to the non-rotating frame, results in three equations for disc-tilt dynamics corresponding to relations A.15 ÷A.17 from the appendix.

7. EXTENDING THE SIX DEGREES OF FREEDOM MODEL TO THE EIGHT DEGREES OF FREEDOM MODEL

The six dof non-linear model is extended to an eight dof model including the first order tip-path-plane equations of motion A.18 ÷ A.20. As demonstrated in [1] this corresponds to taking into account the low frequency regressing flapping mode on top of the steady-state tip-path plane solution. A formal representation of the extension of the six dof model to the eight dof model is:

$$\begin{bmatrix} I & Body\text{-}Rotor^I \\ Rotor^I\text{-}Body & Rotor^I\text{-}Rotor^I \end{bmatrix}\begin{bmatrix}\dot{u}\\ \cdot\\ \cdot\\ \dot{r}\\ \dot{a}_0\\ \dot{a}_1\\ \dot{b}_1\end{bmatrix}= \begin{bmatrix} Body\text{-}Body & Body\text{-}Rotor^I \\ Rotor^I\text{-}Body & Rotor^I\text{-}Rotor^{s.s} \end{bmatrix}\begin{bmatrix}u\\ \cdot\\ \cdot\\ r\\ a_0\\ a_1\\ b_1\end{bmatrix} \qquad (14)$$

Relation (14) shows that the eight dof model includes a "body-to-rotor first-order disc-tilt dynamics" coupling as well as a "rotor-to-body first -order disc-tilt dynamics" coupling.

7.1 Flying the deceleration manoeuvre with the non-linear eight degrees of freedom model

The deceleration manoeuvre is now simulated first with the Bo105 helicopter and then with the Puma helicopter, using the eight dof non-linear model presented above, in order to account for the effects of the first order disc-tilt dynamics on the piloted simulation model.

Deceleration manoeuvre: Bo105

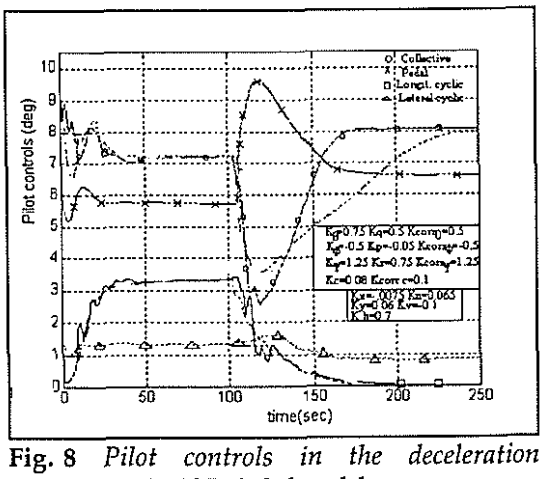

Fig. 8 *Pilot controls in the deceleration manoeuvre, Bo105, 8 dof model*

Comparing fig 8 and fig 3 it is clear that the pilot has difficulties in performing the manoeuvre with the gains deducted in the six dof model.

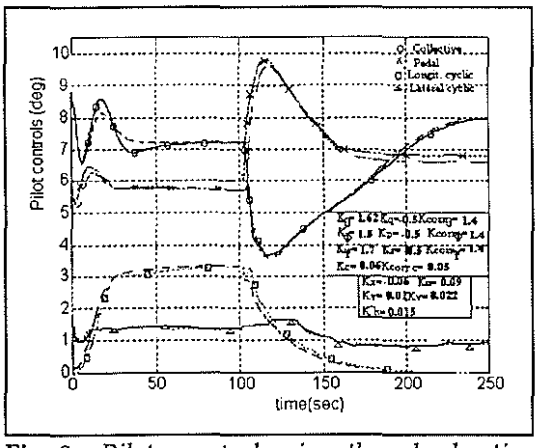

Fig. 9 *Pilot controls in the deceleration manoeuvre with Bo105, 8 dof model, new gains*

Therefore, the gains are adjusted so that the pilot can easier perform the manoeuvre. The results are shown in fig.9. From this figure, it can be seen that the pilot gives inputs with different amplitude, justifying the conclusion that the flapping influences the piloted simulation model of Bo105.

Deceleration manoeuvre: Puma

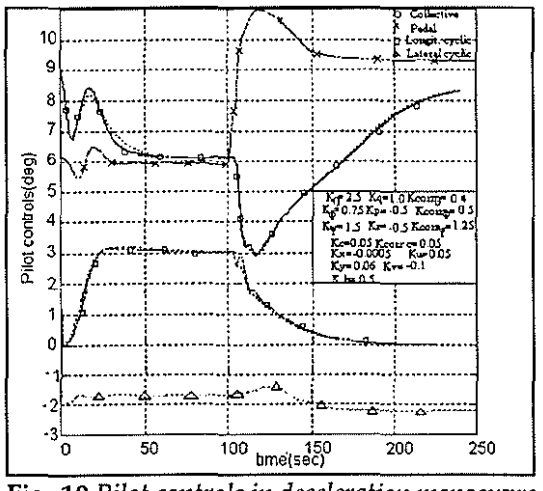

Fig. 10 *Pilot controls in deceleration manoeuvre with Puma, 8 dof model*

Comparing fig. 10 with fig 4 the differences between the results of the 6 and 8 dof model are hardly visible. This leads to the conclusion that the flapping dynamics does not influence pilot controls in case of the Puma helicopter.
Therefore, one may expect that a model including the first order tip-path plane dynamics is needed for the Bo105, as opposed to the Puma, where flapping dynamics did not influence the pilot model.

7.2 Flying the side-step manoeuvre with the non-linear eight degrees of freedom model

The second manoeuvre chosen as example in this paper is now simulated using the eight dof model, again first with the Bo105 and then with the Puma helicopter.

Side-step manoeuvre: Bo105

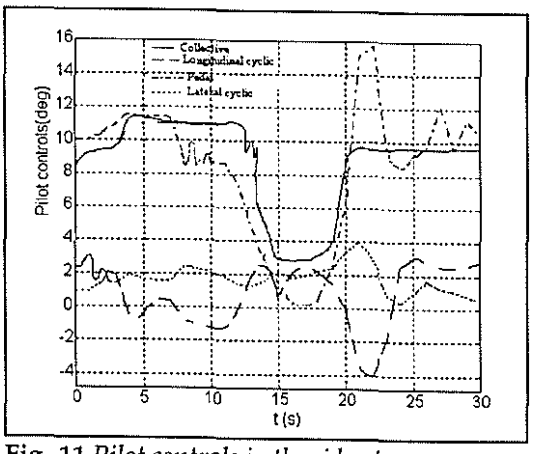

Fig. 11 *Pilot controls in the side-step manoeuvre with Bo105, 8 dof model*

Gains used:

K_Θ=2.3 K_q=-0.57 $K_{corr\,\Theta}$=1.43
K_Φ=-0.5 K_p=-0.57 $K_{corr\,\Phi}$=1.43
K_Ψ=1.23 K_r=-0.57 $K_{corr\,\Psi}$=1.43
K_c=0.1 $K_{corr\,c}$=0.05
K_x=--0.06 K_u=0.09
K_y=0.06 K_v=0.0225
K_h=0.08

As in the case of the deceleration manoeuvre with the Bo105, the gains had to be changed in order to simulate the side-step manoeuvre. The new gains and the resulted pilot actions are given above. Again, it can be seen that the first-order tip-path plane influences the pilot model.

Side-step manoeuvre: Puma

Comparing fig. 12 with fig 7 , the gains can still be kept to the values used in the 6 dof model, but the inputs are now quite different in amplitude comparing to those in the 6 dof model. It was also tried to get results closer to the 6 dof model by changing the gains, but the differences were even bigger. Therefore, one can conclude that the first order flapping dynamics influences the way a pilot

flies the side-step manoeuvre with the Puma helicopter.

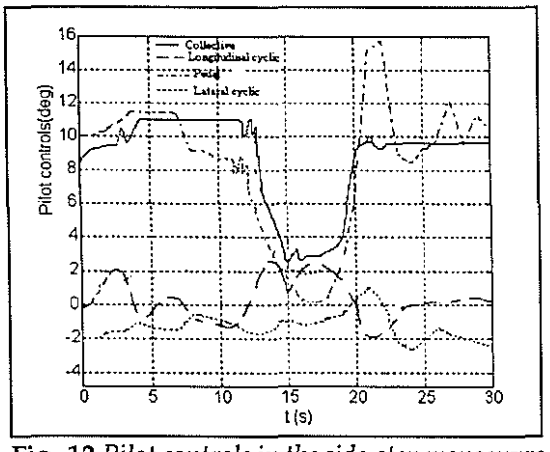

Fig. 12 *Pilot controls in the side-step manoeuvre with Puma, 8 dof model*

8. EXTENDING THE SIX DEGREES OF FREEDOM MODEL TO THE NINE DEGREES OF FREEDOM MODEL

The six dof model is extended to the nine dof model in order to account for the influence of all transient flapping blade motion. This is done by including the complete flapping equations of motion A.15÷A.17.

These second- order differential equations are then transformed into first order differential equations, resulting in six degrees of freedom for the flapping motion. The newly developed model is the so-called "nine dof model".

This model considers, as far as the flapping motion is concerned, on top of the steady state solution, the first order tip-path-plane motion as in the eight dof model and also the second order tip-path plane motion.

The extension of the six dof model to the nine dof model is formally represented in (15), showing that there two levels of couplings now: firstly between the body and the first-order disc-tilt dynamics, identical to that of the eight dof model, and secondly between the body and the second-order disc-tilt dynamics, and vice-versa.

$$\begin{bmatrix} I & \text{Body-Rotor}^{I} & \text{Body-Rotor}^{II} \\ 0 & I & 0 \\ \text{Rotor}^{II}\text{-Body} & \text{Rotor}^{II}\text{-Rotor}^{I} & I \end{bmatrix} \begin{bmatrix} \dot{u} \\ \dot{r} \\ \dot{a}_0 \\ \dot{b}_1 \\ \dot{a}_0 \\ \dot{b}_1 \end{bmatrix} - \begin{bmatrix} \text{Body-Body} & \text{Body-Rotor}^{I} & \text{Body-Rotor}^{II} \\ 0 & 0 & I \\ \text{Rotor}^{II}\text{-Body} & \text{Rotor}^{II}\text{-Rotor}^{II} & I \end{bmatrix} \begin{bmatrix} u \\ r \\ a_0 \\ b_1 \\ a_0 \\ b_1 \end{bmatrix} \tag{15}$$

8.1 Flying the deceleration manoeuvre with the non-linear nine degrees of freedom model

As a final step in the investigation of the influence of the flapping dynamics on the helicopter piloted simulation model, the deceleration manoeuvre is simulated with the Bo105 helicopter including all the transient flapping motions in the model as given by the nine dof model.

Deceleration manoeuvre: Bo105

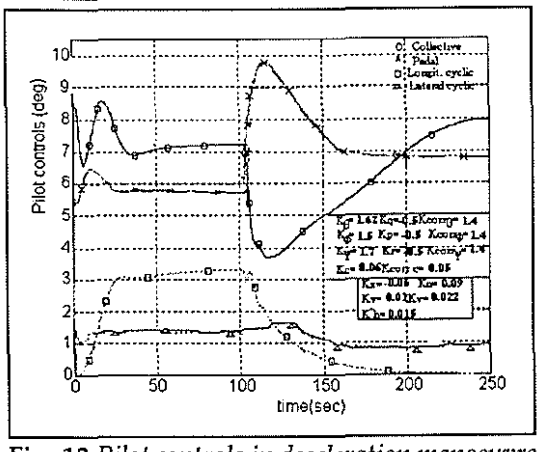

Fig. 13 *Pilot controls in deceleration manoeuvre with Bo105, 9 dof model*

Comparing fig 13 and fig 8, one can observe that there is no influence of the tip-path-plane flapping accelerations on simulating the manoeuvre.

Deceleration manoeuvre: Puma

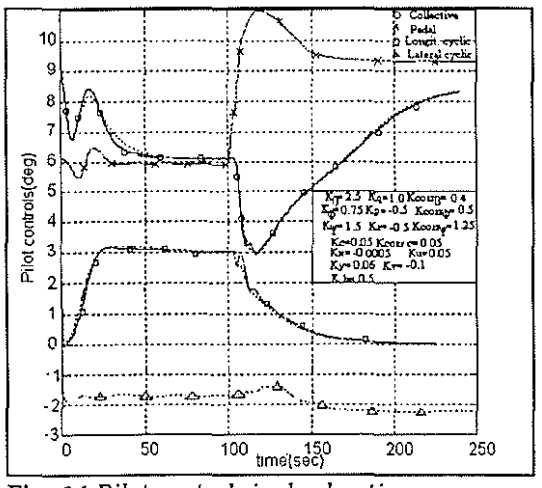

Fig. 14 *Pilot controls in deceleration manoeuvre with Puma, 9 dof model*

For the Puma, one can already expect that using the second-order tip-path plane equations of motion, there is no difference in the way the pilot flies the deceleration manoeuvre since it was already shown that the first order flapping dynamics does not influenced the piloted simulation.

9. INVESTIGATIONS IN THE COMPLEX PLANE

Reference [1] presented an investigation in the complex plane applied in order to determine the necessary degrees of freedom in a piloted simulation model. The method was then exemplified for the rigid blade flapping. It was found that the regressing mode of the Bo105 was much closer to the short period than the one found for the Puma. This chapter investigates the way in which the body short period moves relative to the regressing flapping mode when simulating the manoeuvres studied in the present paper.

9.1 Deceleration manoeuvre in "the complex plane": Bo105

Analysing fig. 15 it can be seen that the short period mode in the six dof model at V=50 m/s is increased in damping and frequency. Changing the gains values in the eight dof model, determines only real values for the eigenvalues of the short period mode. The eigenvalues of the regressing flapping mode do not shift in the complex plane because only the representation of the uncoupled flapping motion has been used.

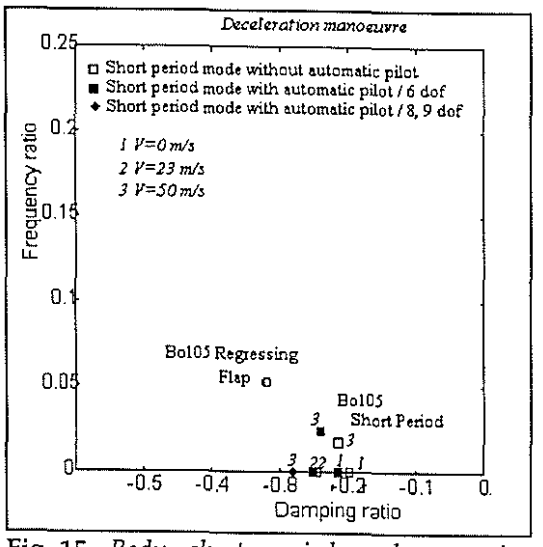

Fig. 15 *Body short period and regressing flapping for the deceleration manoeuvre: Bo105*

9.2 Deceleration manoeuvre in "the complex plane": Puma

For the Puma helicopter, the gains used in the six dof model could also be kept constant in the eight and nine dof model. Looking at fig.16 it can be seen that the short period mode in the six dof model with the automatic pilot has only real eigenvalues.

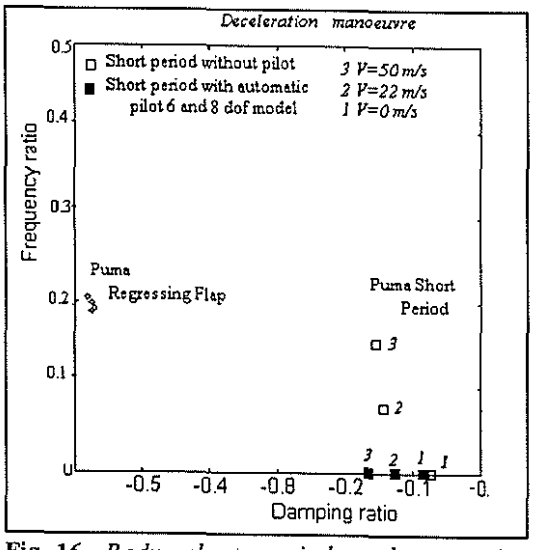

Fig. 16 *Body short period and regressing flapping for the deceleration manoeuvre: Puma*

9.3 Side-step manoeuvre "in the complex plane": Bo105

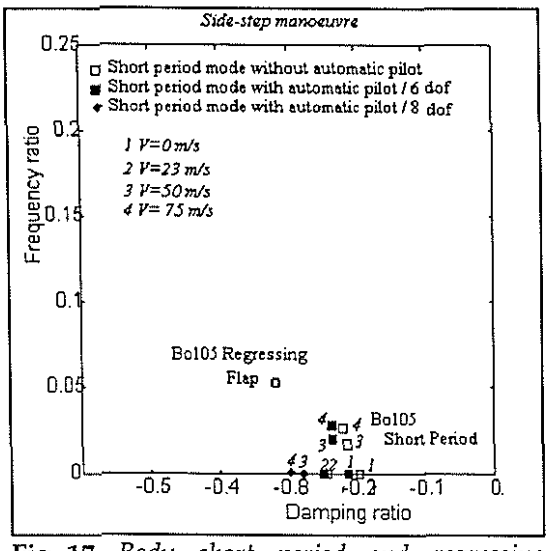

Fig. 17 *Body short period and regressing flapping for the side-step manoeuvre: Bo105*

As for the deceleration manoeuvre, the eigenvalues of the short period mode in the six dof model for the side-step manoeuvre with the automatic pilot, are complex values for velocities higher than 50m/s. Changing the gains in the eight dof model, the eigenvalues of the short period mode become real.

9.4 Side-step manoeuvre "in the complex plane": Puma

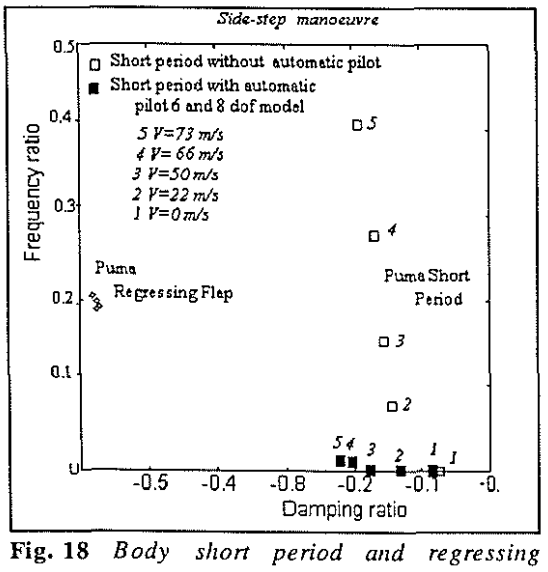

Fig. 18 *Body short period and regressing flapping for the side-step manoeuvre: Puma*

In the case of the side-step manoeuvre with the automatic pilot performed with Puma helicopter, the eigenvalues of the short period mode are still complex values, but their frequency is much low that the values obtained without the automatic pilot.

10. INFLUENCE OF DIFFERENT APPROXIMATIONS FOR THE STEADY-STATE FLAPPING ANGLES ON FLYING THE MANOEUVRES

Considering the same assumptions in deriving the flapping motion in the rotating frame as explained in paragraph 6, the flapping blade equation of motion is derived, this time without neglecting the higher order terms appearing in the equations of motion. The blade flapping equation of motion (10) becomes:

$$\frac{\ddot{\beta}}{\Omega^2}+\beta\left(\nu^2-2\bar{r}+\bar{r}^2-\bar{p}^2\cos^2\psi+2\bar{p}\bar{q}\cos\psi\sin\psi-\right.$$
$$\left.-\bar{q}^2\sin\psi\right)=2\bar{p}\cos\psi-2\bar{q}\sin\psi-\bar{r}\bar{p}\cos\psi+\bar{r}\bar{q}\sin\psi+$$
$$+\frac{M_a}{I_{bl}\Omega^2} \qquad (16)$$

and the air velocities are now:

$$\bar{U}_T=\frac{u}{\Omega R}\sin\psi+\frac{v}{\Omega R}\cos\psi+\bar{r}_{bl}(1-\bar{r})+\bar{r}_{bl}\beta\times \qquad (17)$$
$$\times(\bar{p}\cos\psi-\bar{q}\sin\psi)-\bar{h}\bar{q}\sin\psi+\bar{h}\bar{p}\cos\psi$$

$$\bar{U}_P=\frac{u}{\Omega R}\beta\cos\psi-\frac{v}{\Omega R}\beta\sin\psi-\frac{w}{\Omega R}-\bar{r}_{bl}\times$$
$$\times\left(\bar{q}\cos\psi+\bar{p}\sin\psi-\frac{\dot{\beta}}{\Omega}\right)+\lambda_0-\bar{h}\bar{q}\beta\cos\psi-\bar{h}\bar{p}\beta\sin\psi$$

Substituting (17) and (18) in (11) and transforming the equation of motion from the rotating plane to the non-rotating frame results in the tip-path plane equations flapping equations. The complete form of these equations is given in [7, pp. 102-103]. Reference [7] presents also a way in which these equations should be simplified [7, pp. 111].

This chapter investigates the influence of three analytical expressions (relations A.21-A.23, relations A.60-A.61 from [7] and relations A.49-A.51 from [7]) on simulating the deceleration manoeuvre with the Bo105. For simulation, the six dof model is used. Fig.19 presents the longitudinal flapping angle (relative to the control plane) of the deceleration manoeuvre calculated using these three analytical expressions. The case of flapping angle without blade twist and flapping hinge offset is also simulated.

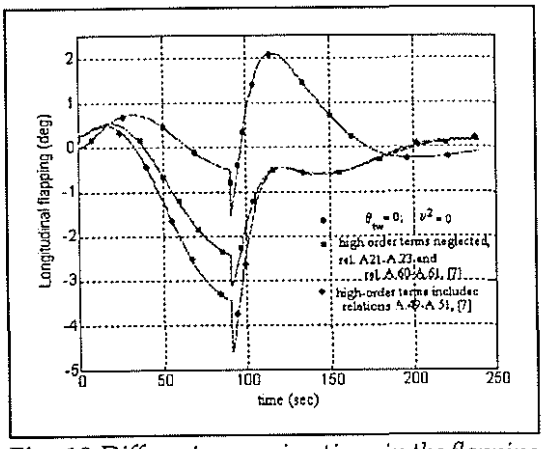

Fig. 19 *Different approximations in the flapping angles, deceleration manoeuvre with Bo105*

From fig. 19 it can be seen that the same results are obtained using formulas A.21-A.23 from this paper, Appendix A, or the relations A.49-A.51, [7]. Retaining the high-order terms and coupling terms in the simulation, it results in different results of the longitudinal flapping angle during the manoeuvre. This result leads to the conclusion that the higher order terms in the analytical expressions of the blade flapping angles influence the simulation results and therefore caution should be expressed in neglecting these terms in the piloted simulation model. This conclusion becomes more true when flying heavy manoeuvres which push the helicopter to its flight limits.

11. CONCLUSIONS

11.1 Conclusions with respect to the disc-tilt dynamics

The paper investigated in the time-domain the effects of the disc-tilt dynamics on the piloted simulation model. Time-domain simulations are performed with three models (a six dof body model, an eight dof first-order disc-tilt dynamics model and a nine dof second order disc-tilt dynamics model) for two different helicopters (Bo105 and Puma SA330) flying two mission tasks (a deceleration and a side-step manoeuvre).

▪ With respect to the first-order disc-tilt dynamics it appeared that:
- flying the deceleration manoeuvre with the Bo105 semi-rigid rotor helicopter, the regressing flapping mode does influence the pilot simulation model,
- flying the deceleration manoeuvre with the Puma articulated rotor helicopter, the regressing flapping mode does not influence the pilot simulation model,
- flying the side-step manoeuvre with the Bo105 semi-rigid rotor helicopter, the regressing flapping mode does influence the pilot simulation model,
- flying the side-step manoeuvre with the Puma articulated rotor helicopter, the regressing flapping mode does influence the pilot simulation model,
These results suggest that the low frequency regressing flapping mode should always be included in the piloted simulation model when analysing a semi-rigid rotor configuration. When analysing an articulated rotor helicopter, the inclusion of the low frequency regressing flapping mode depends on the manoeuvre analyzed.

▸ With respect to the second-order disc-tilt dynamics it followed that:
- flying the deceleration manoeuvre with the Bo105 semi-rigid rotor helicopter, the high frequency advancing flapping mode does not influence the pilot simulation model,
- flying the deceleration manoeuvre with the Puma articulated rotor helicopter, the high frequency advancing flapping mode does not influence the pilot simulation model.
These results suggest that the high frequency advancing flapping mode does not need to be included in the model, for the semi-rigid rotor helicopter nor for the articulated rotor helicopter.

11.2 Conclusions with respect to the analytical expressions of the steady-state flapping angles

The paper showed also the influence on the piloted simulation model of the high order terms and couplings from the analytical expressions of the steady-state flapping angles. Simulating the deceleration manoeuvre using different approximations in the flapping angles, it followed that these terms are influencing the piloted model. Therefore, although the high order terms are usually neglected, caution should be expressed as to their influence on the piloted simulation model.

12. RECOMMENDATIONS

The present investigation was carried out having as final goal in mind to obtain a formal procedure which is able to predict the necessary level of detail in the piloted simulation model. As a first step, the body-flap coupling was investigated. Some recommendations on how to continue in the future can be made.

- knowing that the uniform inflow leads to significant errors in the lateral flap motion [4,pp. 205], time-domain simulations should be performed

with model that include the non-uniform inflow,

- in order to be able to develop criteria in the complex plane relative to the level of detail necessary in the piloted simulation model, further time-domain simulations should be performed with other typical cases (different rotor parameters, aerodynamic models, different manoeuvres)

REFERENCES

1. M.D. Pavel, Th. van Holten, "On the Prediction of the Necessary Rotor Dynamics for Helicopter Flight Simulation", 23rd European Rotorcraft Forum, Dresden, Duitsland, September 1997, paper No.39

2. Marinescu, A, Anghel, V., "Aerodinamica si Dinamica Elicopterului", Academy Press, 1992, in Romanian

3. van Holten, Th., Melkert, K.A., "Prestaties en Vliegeigenschappen van Hefschroefvliegtuigen", Technical University Delft, 1994, in Dutch

4. Johnson, W., "Helicopter Theory", Dover Publications Inc., 1994

5. Chen, R. T.N., "A Simplified Rotor System Mathematical Model for Piloted Flight Dynamics Simulation", NASA TM-78575, May, 1979

6. Pavel, M.D., "Prediction of the Necessary Flapping Dynamics for Helicopter Flight Simulation", M-757, TU Delft, Dec. 1996

7. Ypma, F.A.K., "On the Prediction of Blade Flapping Angles", M-730, TU Delft, Dec. 1996

8. Hommel, G.C.S., "Effects of Rotor Flapping Dynamics on Helicopter Flight Simulation", M.Sc. Thesis, Oct. 1997

9. Curtiss, H.C. Jr., Shupe, N.K., "A Stability and Control Theory for Hingeless Rotors", 27th Annual National Forum of the American Helicopter Society, May, 1971,

10. Hohenemser, K.H., Yin, S.K., "Methods Studies Toward Simplified Rotor-Body Dynamics", Part I of First Yearly Report under Contract NAS2-7613, June 1974

APPENDIX A- EQUATIONS OF MOTION SIX DEGREES OF FREEDOM BODY MODEL

Appendix A gives the equations of motion of the six degrees of freedom non-linear piloted model developed in the present paper.

Nomenclature

I_x	helicopter moment of inertia about body x-axis [kg m^2]
I_y	helicopter moment of inertia about body y-axis [kg m^2]
I_z	helicopter moment of inertia about body z-axis [kg m^2]
I_{xz}	helicopter product of inertia about body x and z-axes [kg m^2]
$p, \bar{p}$	helicopter roll angular velocity [rad/s] and its non-dimensional value [-]
$q, \bar{q}$	helicopter pitch angular velocity [rad/s] and its non-dimensional value [-]
$r, \bar{r}$ r	helicopter yaw angular velocity [rad/s] and its non-dimensional value [-]
m	helicopter mass [kg]
u	component of airspeed along body x-axis [m/s]
v	component of airspeed along body y-axis [m/s]
w	component of airspeed along body z-axis [m/s]
V	total helicopter velocity [m/s]
x	position along Earth X-axis [m]
y	position along Earth Y-axis [m]
z	position along Earth Z-axis [m]
$\mu_x = u/(\Omega R)$	normalised velocity component along x-axis [-]
$\mu_y = v/(\Omega R)$	normalised velocity component along y-axis [-]
$\mu_z = w/(\Omega R)$	normalised velocity component along z-axis [-]
Θ	Euler pitch angle [rad]
Ψ	heading angle [rad]
Φ	Euler roll angle [rad]
c	helicopter climb velocity [m/s]
h	helicopter altitude [m]

Rotor

a_0	coning angle [rad]
a_1	longitudinal flapping angle [rad]; $a_1>0$ if the tip-path plane tilts backwards
b_1	lateral flapping angle [rad] $b_1>0$ for tilting to the right (ψ=90 deg)
$\beta = a0 - a_1\cos\psi - b_1\sin\psi$	blade flapping angle [rad]
C_l^{α}	blade lift curve slope [rad^{-1}]
$C_d = 0.011 + 0.4(\alpha - a_1)$	blade drag coefficient
C_t	thrust coefficient relative to the disc plane [-]
C_t^{elem}	thrust coefficient calculated with the blade-element theory
C_t^{gl}	thrust coefficient calculated with the Glauert theory
C_H	rotor drag force coefficient [-]
C_S	rotor lateral force coefficient [-]
C_Q	rotor torque coefficient [-]
I_bl	inertia moment of the blade section (m^4)
K_β	flap hinge spring constant
m_{bl}	blade mass (kg)
e, ε	flapping hinge offset [m] and its non-dimensional value [-]
N	number of rotor blades [-]
R	rotor radius [m]

$T=\rho(\Omega R)^2(\pi R^2)C_t$	rotor thrust
$H=\rho(\Omega R)^2(\pi R^2)C_H$	rotor drag force
$S=\rho(\Omega R)^2(\pi R^2)C_S$	rotor lateral force
$Q=\rho(\Omega R)^2(\pi R^2)RC_Q$	rotor torque
$D=\frac{\rho}{2}V^2SC_d$	blade drag force
$(Vol_{fus})_m = \frac{\pi}{4}\int_0^{l_f} d_f^2(x)\,dx$	volume of a body equivalent to the fuselage having only circular sections [m^3]
$M_{fus}=\rho V^2 K_{fus}(Vol_{fus})_m \alpha_{sp}$	fuselage pitch moment [Nm]
(x_h, y_h, z_h)	position of the rotor hub relative to the body-axes system
α	rotor incidence [rad] relative to no-feathering plane
γ	Lock number
λ_0	normalised uniform inflow velocity [-]
$\lambda=-\mu_z+\lambda_0$	
$\nu^2=1+K_\beta/(I_b\Omega^2)$	non-dimensional natural frequency of the flap motion
σ	rotor solidity (plenitude coefficient)
ψ	azimuth angle [rad]
θ_0	collective pitch [rad]
θ_{1c}	lateral cyclic pitch [rad] $\theta_{1c}>0$ for pilot stick to the right
θ_{1s}	longitudinal cyclic pitch [rad] $\theta_{1s}>0$ for stick forwards
θ_{tw}	blade twist [rad]
$\theta=\theta_0+\theta_{tw}-\theta_{1c}\cos\psi-\theta_{1s}\sin\psi$	blade pitch angle [rad]
Ω	rotor rotational speed [rad/sec]
Tailrotor	
C_{tr}	tailrotor thrust coefficient [-]
$f_{tr}=1-3S_{fin}/(4\pi R_{tr}^2)$	tailrotor fin blockage factor [-]
R_{tr}	tailrotor radius [m]
(x_{tr}, z_{tr})	tailrotor position relative to the helicopter body-axis system
Ω_{tr}	tailrotor speed [rad/sec]
$k_{tr}=1$	main rotor downwash factor at tailrotor
$\mu_{xtr}=\frac{\sqrt{u^2+(w+k_{tr}\Omega R\lambda_0+qx_{tr})^2}}{\Omega_{tr}R_{tr}}$	normalized tailrotor velocity along x-axis [-]
$\mu_{ztr}=-\frac{v-rx_{tr}+pz_{tr}}{\Omega_{tr}R_{tr}}$	normalized tailrotor velocity along z-axis [-]
$\lambda_{0\,tr}$	normalized tailrotor uniform inflow velocity
θ_{0tr}	tailrotor collective [rad]
$T_{tr}=\rho(\Omega_{tr}R_{tr})^2(\pi R_{tr}^2)C_{t\,tr}$	tailrotor thrust
Vertical fin	
(x_{fin}, z_{fin})	position of the vertical fin relative to the body-axes system
S_{fin}	fin area [m^2]

$V_{fin}=\sqrt{u^2+(v-rx_{fin}+pz_{fin})^2}$ vertical fin velocity [m/s]

β_{0fin} vertical fin incidence

$\beta_{fin}=\beta_{0fin}+\arctan\left(\frac{v-rx_{fin}+pz_{fin}}{u}\right)$ vertical fin incidence [m/s]

$Lift_{fin}=\frac{\rho}{2}S_{fin}V_{fin}^2C_{lfin}^{\beta}\beta_{fin}$ vertical fin lift force

Horizontal stabilizer

(x_{hs}, z_{hs}) horizontal stabilizer position relative to the body-axes system

S_{hs} horizontal stabilizer area [m^2]

$V_{hs}=\sqrt{u^2+(w+qx_{hs})^2}$ horizontal stabilizer velocity [m/s]

α_{0hs} horizontal stabilizer incidence

$\alpha_{hs}=\alpha_{0hs}+\arctan\left(\frac{w+qx_{hs}}{u}\right)$ horizontal stabilizer incidence

$Lift_{hs}=\frac{\rho}{2}S_{hs}V_{hs}^2C_{lhs}^{\alpha}\alpha_{hs}$ horizontal stabilizer lift force

Body equations of motion

$$\dot{u}=-g\sin\Theta-\frac{T}{m}\sin(a_1-\theta_{1s})\cos(b_1+\theta_{1c})-\frac{H}{m}\cos(a_1-\theta_{1s})+\frac{S}{m}\sin(a_1-\theta_{1s})\sin(b_1+\theta_{1c})-\frac{D}{m}\frac{u}{v}+rv-qw \quad (A.1)$$

$$\dot{v}=g\sin\Theta\sin\Phi+\frac{T}{m}\sin(b_1+\theta_{1c})+\frac{S}{m}\cos(b_1+\theta_{1c})+\frac{T_{tr}}{m}f_{tr}-\frac{Lift_{fin}}{m}-ru+pw \quad (A.2)$$

$$\dot{w}=g\cos\Theta\cos\Phi-\frac{T}{m}\cos(a_1-\theta_{1s})\cos(b_1+\theta_{1c})+\frac{H}{m}\sin(a_1-\theta_{1s})+\frac{S}{m}\cos(a_1-\theta_{1s})\sin(b_1+\theta_{1c})-\frac{D}{m}\frac{w}{V}-\frac{Lift_{hs}}{m}-pv+qu \quad (A.3)$$

$$\dot{p}=\frac{T}{I_x}\left(z_h\sin(b_1+\theta_{1c})+y_h\cos(a_1-\theta_{1s})\cos(b_1+\theta_{1c})\right)-\frac{H}{I_x}y_h\sin(a_1-\theta_{1s})+\frac{S}{I_x}\left(z_h\cos(b_1+\theta_{1c})-y_h\cos(a_1-\theta_{1s})\sin(b_1+\theta_{1c})\right)+$$
$$+\frac{T_{tr}}{I_x}z_{tr}f_{tr}-\frac{Lift_{fin}}{I_x}z_{fin}+\frac{m_{bl}}{I_x}e\Omega^2R^2\sin(b_1+\theta_{1c})+\frac{-(I_z-I_y)qr+(\dot{r}+pq)I_{xz}}{I_x} \quad (A.4)$$

$$\dot{q}=\frac{T}{I_y}\left(z_h\sin\left(a_1-\theta_{1s}\right)\cos\left(b_1+\theta_{1c}\right)+x_h\cos\left(a_1-\theta_{1s}\right)\cos\left(b_1+\theta_{1c}\right)\right)+\frac{H}{I_y}\left(z_h\cos\left(a_1-\theta_{1s}\right)-x_h\cos\left(a_1-\theta_{1s}\right)\right)-\frac{S}{I_y}\left(z_h\sin\left(a_1-\theta_{1s}\right)\sin\left(b_1+\theta_{1c}\right)+\right.$$
$$+\frac{M_{fus}}{I_y}-\frac{Lift_{hs}}{I_y}x_{hs}+\frac{m_{bl}}{I_y}e\,\Omega^2R^2\sin\left(a_1-\theta_{1s}\right)+\frac{-(I_x-I_z)pr-(p^2-r^2)I_{xz}}{I_y} \tag{A.5}$$

$$\dot{r}=\frac{Q}{I_z}-\frac{T}{I_z}\left(y_h\sin\left(a_1-\theta_{1s}\right)\cos\left(b_1+\theta_{1c}\right)+x_h\sin\left(b_1+\theta_{1c}\right)\right)-\frac{H}{I_z}y_h\cos\left(a_1-\theta_{1s}\right)+\frac{S}{I_z}\left(y_h\sin\left(a_1-\theta_{1s}\right)\sin\left(b_1+\theta_{1c}\right)-x_h\cos\left(b_1+\theta_{1c}\right)\right)-$$
$$-\frac{T_{tr}}{I_z}x_{tr}f_{tr}+\frac{Lift_{fin}}{I_z}x_{fin}+\frac{-(I_y-I_x)pq+(\dot{p}-rq)I_{xz}}{I_z} \tag{A.6}$$

$$\dot{\Phi}=p+(q\sin\Phi+r\cos\Phi)\tan\Theta \tag{A.7}$$

$$\dot{\Theta}=q\cos\Phi-r\sin\Phi \tag{A.8}$$

$$\dot{\Psi}=\frac{q\sin\Psi+r\cos\Phi}{\cos\Theta} \tag{A.9}$$

$$\dot{x}=[u\cos\Theta+(v\sin\Phi+w\cos\Phi)\sin\Theta)]\cos\Psi-(v\cos\Phi-w\sin\Phi)\sin\Psi \tag{A.10}$$

$$\dot{y}=[u\cos\Theta+(v\sin\Phi+w\cos\Phi)\sin\Theta)]\sin\Psi+(v\cos\Phi-w\sin\Phi)\cos\Psi \tag{A.11}$$

$$\dot{z}=-u\sin\Theta+(v\sin\Phi+w\cos\Phi)\cos\Theta \tag{A.12}$$

$$\tau_{\lambda_0}\dot{\lambda}_0=C_t^{elem}-C_t^{gl} \tag{A.13}$$

$$\tau_{\lambda_{0_{tr}}}\dot{\lambda}_{0_{tr}}=C_{t_{tr}}^{elem}-C_{t_{tr}}^{gl} \tag{A.14}$$

Second Order Flapping Disc-Tilt Dynamics

$$\frac{\ddot{a}_0}{\Omega^2}+\frac{\gamma}{8}(1-\bar{r})\frac{\dot{a}_0}{\Omega}-\frac{\gamma}{12}\mu_x\frac{\dot{b}_1}{\Omega}-\frac{\gamma}{12}\mu_y\frac{\dot{a}_1}{\Omega}+\left(\nu^2-2\bar{r}\right)a_0=\frac{\gamma}{8}\left(1+\mu_x^2-2\bar{r}\right)\theta_0-\frac{\gamma}{6}\mu_y\theta_{1c}-\frac{\gamma}{6}\mu_x\theta_{1s}+\frac{\gamma}{8}\left(\frac{4}{5}-\frac{8}{5}\bar{r}+\frac{2}{3}\mu_x^2\right)\theta_{tw}-$$
$$-\frac{\gamma}{6}(-\mu_z+\lambda_0)+\frac{\gamma}{12}\mu_x\bar{p}+\frac{\gamma}{12}\mu_y\bar{q} \tag{A.15}$$

$$\frac{\ddot{a}_1}{\Omega^2}-\frac{\gamma}{8}(1-\bar{r})\frac{\dot{a}_1}{\Omega}+\frac{\gamma}{6}\mu_y\frac{\dot{a}_0}{\Omega}-2\frac{\dot{b}_1}{\Omega}+\frac{\gamma}{6}\mu_x a_0+\left(1-v^2+2\bar{r}\right)a_1+\frac{\gamma}{8}\left(-1+\bar{r}-\frac{\mu_x^2}{2}+\frac{\mu_y^2}{2}\right)b_1=\frac{\gamma}{3}\mu_y\theta_0-\frac{\gamma}{8}\left(1-2\bar{r}+\frac{\mu_x^2}{2}\right)\theta_{1c}-$$
$$-\frac{\gamma}{8}\mu_x\mu_y\theta_{1s}+\frac{\gamma}{4}\mu_y\theta_{tw}-\frac{\gamma}{8}\mu_y(-\mu_z+\lambda_0)+2\bar{p}+\frac{\gamma}{8}\bar{q} \qquad \text{(A.16)}$$

$$\frac{\ddot{b}_1}{\Omega^2}+\gamma\frac{\mu_x}{6}\frac{\dot{a}_0}{\Omega}+2\frac{\dot{a}_1}{\Omega}-\frac{\gamma}{8}(1-\bar{r})\frac{\dot{b}_1}{\Omega}+\frac{\gamma}{6}\mu_y a_0-\frac{\gamma}{8}\left(1-\bar{r}-\frac{\mu_x^2}{2}+\frac{\mu_y^2}{2}\right)a_1-\left(1-v^2+2\bar{r}\right)b_1=-\frac{\gamma}{3}\mu_x\theta_0+\frac{\gamma}{8}\mu_x\mu_y\theta_{1c}+$$
$$+\frac{\gamma}{8}\left(1-2\bar{r}+\frac{3}{2}\mu_x^2\right)\theta_{1s}-\frac{\gamma}{4}\mu_x\theta_{tw}+\frac{\gamma}{4}\mu_x(-\mu_z+\lambda_0)-\frac{\gamma}{8}\bar{p}+2\bar{q} \qquad \text{(A.17)}$$

First Order Flapping Disc-Tilt Dynamics

$$\frac{\gamma}{8}(1-\bar{r})\frac{\dot{a}_0}{\Omega}-\frac{\gamma}{12}\mu_x\frac{\dot{b}_1}{\Omega}-\frac{\gamma}{12}\mu_y\frac{\dot{a}_1}{\Omega}+\left(v^2-2\bar{r}\right)a_0=\frac{\gamma}{8}\left(1+\mu_x^2-2\bar{r}\right)\theta_0-\frac{\gamma}{6}\mu_y\theta_{1c}-\frac{\gamma}{6}\mu_x\theta_{1s}+\frac{\gamma}{8}\left(\frac{4}{5}-\frac{8}{5}\bar{r}+\frac{2}{3}\mu_x^2\right)\theta_{tw}-$$
$$-\frac{\gamma}{6}(-\mu_z+\lambda_0)+\frac{\gamma}{12}\mu_x\bar{p}+\frac{\gamma}{12}\mu_y\bar{q} \qquad \text{(A.18)}$$

$$-\frac{\gamma}{8}(1-\bar{r})\frac{\dot{a}_1}{\Omega}+\frac{\gamma}{6}\mu_y\frac{\dot{a}_0}{\Omega}-2\frac{\dot{b}_1}{\Omega}+\frac{\gamma}{6}\mu_x a_0+\left(1-v^2+2\bar{r}\right)a_1+\frac{\gamma}{8}\left(-1+\bar{r}-\frac{\mu_x^2}{2}+\frac{\mu_y^2}{2}\right)b_1=\frac{\gamma}{3}\mu_y\theta_0-\frac{\gamma}{8}\left(1-2\bar{r}+\frac{\mu_x^2}{2}\right)\theta_{1c}-$$
$$-\frac{\gamma}{8}\mu_x\mu_y\theta_{1s}+\frac{\gamma}{4}\mu_y\theta_{tw}-\frac{\gamma}{8}\mu_y(-\mu_z+\lambda_0)+2\bar{p}+\frac{\gamma}{8}\bar{q} \qquad \text{(A.19)}$$

$$\gamma\frac{\mu_x}{6}\frac{\dot{a}_0}{\Omega}+2\frac{\dot{a}_1}{\Omega}-\frac{\gamma}{8}(1-\bar{r})\frac{\dot{b}_1}{\Omega}+\frac{\gamma}{6}\mu_y a_0-\frac{\gamma}{8}\left(1-\bar{r}-\frac{\mu_x^2}{2}+\frac{\mu_y^2}{2}\right)a_1-\left(1-v^2+2\bar{r}\right)b_1=-\frac{\gamma}{3}\mu_x\theta_0+\frac{\gamma}{8}\mu_x\mu_y\theta_{1c}+$$
$$+\frac{\gamma}{8}\left(1-2\bar{r}+\frac{3}{2}\mu_x^2\right)\theta_{1s}-\frac{\gamma}{4}\mu_x\theta_{tw}+\frac{\gamma}{4}\mu_x(-\mu_z+\lambda_0)-\frac{\gamma}{8}\bar{p}+2\bar{q} \qquad \text{(A.20)}$$

Steady-state Flapping Angles

$$\left(v^2-2\bar{r}\right)a_0=\frac{\gamma}{8}\left(1+\mu_x^2-2\bar{r}\right)\theta_0-\frac{\gamma}{6}\mu_y\theta_{1c}-\frac{\gamma}{6}\mu_x\theta_{1s}+\frac{\gamma}{8}\left(\frac{4}{5}-\frac{8}{5}\bar{r}+\frac{2}{3}\mu_x^2\right)\theta_{tw}-\frac{\gamma}{6}(-\mu_z+\lambda_0)+\frac{\gamma}{12}\mu_x\bar{p}+\frac{\gamma}{12}\mu_y\bar{q} \qquad \text{(A.21)}$$

$$\frac{\gamma}{8}\left(1-\bar{r}-\frac{\mu_x^2}{2}+\frac{\mu_y^2}{2}\right)a_1=\frac{\gamma}{6}\mu_y a_0+\left(v^2-1-2\bar{r}\right)b_1+\frac{\gamma}{3}\mu_x\theta_0-\frac{\gamma}{8}\mu_x\mu_y\theta_{1c}-\frac{\gamma}{8}\left(1-2\bar{r}+\frac{3}{2}\mu_x^2\right)\theta_{1s}+$$
$$+\frac{\gamma}{4}\mu_x\theta_{tw}-\frac{\gamma}{4}\mu_x(-\mu_z+\lambda_0)+\frac{\gamma}{8}\bar{p}-2\bar{q} \qquad \text{(A.22)}$$

$$\frac{\gamma}{8}\left(-1+\bar{r}-\frac{\mu_x^2}{2}+\frac{\mu_y^2}{2}\right)b_1=-\frac{\gamma}{6}\mu_x a_0+\left(v^2-1-2\bar{r}\right)a_1\frac{\gamma}{3}\mu_y\theta_0-\frac{\gamma}{8}\left(1-2\bar{r}+\frac{\mu_x^2}{2}\right)\theta_{1c}-\frac{\gamma}{8}\mu_x\mu_y\theta_{1s}+$$
$$+\frac{\gamma}{4}\mu_y\theta_{tw}-\frac{\gamma}{8}\mu_y(-\mu_z+\lambda_0)+2\bar{p}+\frac{\gamma}{8}\bar{q} \qquad \text{(A.23)}$$